

# First results on nucleon resonance photocouplings from the $\gamma p \rightarrow \pi^+ \pi^- p$ reaction

E. Golovatch<sup>ai,\*</sup>, V.D. Burkert<sup>al</sup>, D.S. Carman<sup>al</sup>, R.W. Gothe<sup>aj</sup>, K. Hicks<sup>ad</sup>, B.S. Ishkhanov<sup>ai</sup>, V.I. Mokeev<sup>al,\*\*</sup>, E. Pasyuk<sup>al,b</sup>, S. Adhikari<sup>m</sup>, Z. Akbar<sup>n</sup>, M.J. Amaryan<sup>ae</sup>, H. Avakian<sup>al</sup>, J. Ball<sup>g</sup>, L. Barion<sup>r</sup>, M. Bashkanov<sup>an</sup>, M. Battaglieri<sup>t</sup>, I. Bedlinskiy<sup>x</sup>, A.S. Biselli<sup>ke</sup>, S. Boiarinov<sup>al</sup>, W.J. Briscoe<sup>p</sup>, F. Cao<sup>i</sup>, A. Celentano<sup>t</sup>, Pierre Chatagnon<sup>w</sup>, T. Chetry<sup>ad</sup>, G. Ciullo<sup>r,l</sup>, L. Clark<sup>ao</sup>, B. A. Clary<sup>i</sup>, P.L. Cole<sup>q</sup>, M. Contalbrigo<sup>r</sup>, V. Crede<sup>n</sup>, A. D'Angelo<sup>u,ah</sup>, N. Dashyan<sup>as</sup>, R. De Vita<sup>t</sup>, E. De Sanctis<sup>s</sup>, M. Defurne<sup>g</sup>, A. Deur<sup>al</sup>, S. Diehl<sup>i</sup>, C. Djalali<sup>aj</sup>, M. Dugger<sup>b</sup>, R. Dupre<sup>w</sup>, H. Egiyan<sup>al</sup>, Mathieu Ehrhart<sup>w</sup>, A. El Alaoui<sup>am</sup>, L. El Fassi<sup>aa</sup>, L. Elouadrhiri<sup>al</sup>, P. Eugenio<sup>n</sup>, G. Fedotov<sup>ad</sup>, R. Fersch<sup>h,ar</sup>, A. Filippi<sup>v</sup>, Y. Ghandilyan<sup>as</sup>, G.P. Gilfoyle<sup>ag</sup>, K.L. Giovanetti<sup>y</sup>, F.X. Girod<sup>al,g</sup>, D.I. Glazier<sup>ao</sup>, K.A. Griffioen<sup>ar</sup>, M. Guidal<sup>w</sup>, L. Guo<sup>m</sup>, K. Hafidi<sup>a</sup>, H. Hakobyan<sup>am,as</sup>, N. Harrison<sup>al</sup>, M. Hattawy<sup>a</sup>, D. Heddle<sup>h,al</sup>, M. Holtrop<sup>ab</sup>, Y. Ilieva<sup>aj,p</sup>, D.G. Ireland<sup>ao</sup>, E.L. Isupov<sup>ai</sup>, D. Jenkins<sup>ap</sup>, H.S. Jo<sup>z,w</sup>, S. Johnston<sup>a</sup>, K. Joo<sup>i</sup>, M.L. Kabir<sup>aa</sup>, D. Keller<sup>aq</sup>, G. Khachatryan<sup>as</sup>, M. Khachatryan<sup>ae</sup>, M. Khandaker<sup>q</sup>, W. Kim<sup>z</sup>, A. Klein<sup>ae</sup>, F.J. Klein<sup>f</sup>, V. Kubarovskiy<sup>al,af</sup>, L. Lanza<sup>u</sup>, P. Lenisa<sup>r</sup>, K. Livingston<sup>ao</sup>, I. J. D. MacGregor<sup>ao</sup>, D. Marchand<sup>w</sup>, N. Markov<sup>i</sup>, B. McKinnon<sup>ao</sup>, C.A. Meyer<sup>e</sup>, R.A. Montgomery<sup>ao</sup>, A. Movsisyan<sup>r</sup>, C. Munoz Camacho<sup>w</sup>, P. Nadel-Turonski<sup>al</sup>, S. Niccolai<sup>w</sup>, G. Niculescu<sup>y</sup>, M. Osipenko<sup>t</sup>, A.I. Ostrovidov<sup>n</sup>, M. Paolone<sup>ak</sup>, R. Paremuzyan<sup>ab</sup>, K. Park<sup>al,z</sup>, O. Pogorelko<sup>x</sup>, J.W. Price<sup>c</sup>, Y. Prok<sup>ae,aq</sup>, D. Protopopescu<sup>ao</sup>, M. Ripani<sup>t</sup>, D. Riser<sup>i</sup>, A. Rizzo<sup>u,ah</sup>, G. Rosner<sup>ao</sup>, F. Sabatié<sup>g</sup>, C. Salgado<sup>ac</sup>, R.A. Schumacher<sup>e</sup>, Y.G. Sharabian<sup>al</sup>, Iu. Skorodumina<sup>aj</sup>, G.D. Smith<sup>an</sup>, D.I. Sober<sup>f</sup>, D. Sokhan<sup>ao</sup>, N. Sparveris<sup>ak</sup>, I.I. Strakovsky<sup>p</sup>, S. Strauch<sup>aj,p</sup>, M. Taiuti<sup>o</sup>, J.A. Tan<sup>z</sup>, N. Tyler<sup>aj</sup>, M. Ungaro<sup>al,i,af</sup>, H. Voskanyan<sup>as</sup>, E. Voutier<sup>w</sup>, R. Wang<sup>w</sup>, X. Wei<sup>al</sup>, M.H. Wood<sup>d,aj</sup>, N. Zachariou<sup>an</sup>, J. Zhang<sup>aq</sup>, Z.W. Zhao<sup>j</sup>, CLAS Collaboration

<sup>a</sup>Argonne National Laboratory, Argonne, Illinois 60439, USA

<sup>b</sup>Arizona State University, Tempe, Arizona 85287-1504

<sup>c</sup>California State University, Dominguez Hills, Carson, CA 90747, USA

<sup>d</sup>Canisius College, Buffalo, NY 14208, USA

<sup>e</sup>Carnegie Mellon University, Pittsburgh, Pennsylvania 15213, USA

<sup>f</sup>Catholic University of America, Washington, D.C. 20064

<sup>g</sup>Irfu/SPHN, CEA, Université Paris-Saclay, 91191 Gif-sur-Yvette, France

<sup>h</sup>Christopher Newport University, Newport News, Virginia 23606, USA

<sup>i</sup>University of Connecticut, Storrs, Connecticut 06269, USA

<sup>j</sup>Duke University, Durham, North Carolina 27708-0305, USA

<sup>k</sup>Fairfield University, Fairfield CT 06824, USA

<sup>l</sup>Università di Ferrara, 44121 Ferrara, Italy

<sup>m</sup>Florida International University, Miami, Florida 33199, USA

<sup>n</sup>Florida State University, Tallahassee, Florida 32306, USA

<sup>o</sup>Università di Genova, 16146 Genova, Italy

<sup>p</sup>The George Washington University, Washington, DC 20052, USA

<sup>q</sup>Idaho State University, Pocatello, Idaho 83209, USA

<sup>r</sup>INFN, Sezione di Ferrara, 44100 Ferrara, Italy

<sup>s</sup>INFN, Laboratori Nazionali di Frascati, 00044 Frascati, Italy

<sup>t</sup>INFN, Sezione di Genova, 16146 Genova, Italy

<sup>u</sup>INFN, Sezione di Roma Tor Vergata, 00133 Rome, Italy

<sup>v</sup>INFN, Sezione di Torino, 10125 Torino, Italy

<sup>w</sup>Institut de Physique Nucléaire, CNRS/IN2P3 and Université Paris Sud, Orsay, France

<sup>x</sup>Institute of Theoretical and Experimental Physics, Moscow, 117259, Russia

<sup>y</sup>James Madison University, Harrisonburg, Virginia 22807

<sup>z</sup>Kyungpook National University, Daegu 41566, Republic of Korea

<sup>aa</sup>Mississippi State University, Mississippi State, MS 39762-5167, USA

<sup>ab</sup>University of New Hampshire, Durham, New Hampshire 03824-3568, USA

<sup>ac</sup>Norfolk State University, Norfolk, Virginia 23504, USA

<sup>ad</sup>Ohio University, Athens, Ohio 45701, USA

<sup>ae</sup>Old Dominion University, Norfolk, Virginia 23529, USA

<sup>af</sup>Rensselaer Polytechnic Institute, Troy, New York 12180-3590, USA

<sup>ag</sup>University of Richmond, Richmond, Virginia 23173, USA

<sup>ah</sup>Università di Roma Tor Vergata, 00133 Rome Italy

<sup>ai</sup>Skobeltsyn Institute of Nuclear Physics and Physics Department, Lomonosov Moscow State University, 119234 Moscow, Russia

<sup>aj</sup>University of South Carolina, Columbia, South Carolina 29208

<sup>ak</sup>Temple University, Philadelphia, PA 19122, USA

<sup>al</sup>Thomas Jefferson National Accelerator Facility, Newport News, Virginia 23606, USA

<sup>am</sup>Universidad Técnica Federico Santa María, Casilla 110-V Valparaíso, Chile

\*Corresponding author

\*\*Principal corresponding author

Email addresses: golovach@jlab.org (E. Golovatch), mokeev@jlab.org (V.I. Mokeev)

<sup>an</sup>Edinburgh University, Edinburgh EH9 3JZ, United Kingdom  
<sup>ao</sup>University of Glasgow, Glasgow G12 8QQ, United Kingdom  
<sup>ap</sup>Virginia Tech, Blacksburg, Virginia 24061-0435, USA  
<sup>aq</sup>University of Virginia, Charlottesville, Virginia 22901, USA  
<sup>ar</sup>College of William and Mary, Williamsburg, Virginia 23187-8795, USA  
<sup>as</sup>Yerevan Physics Institute, 375036 Yerevan, Armenia

---

## Abstract

We report the first experimental measurements of the nine 1-fold differential cross sections for the  $\gamma p \rightarrow \pi^+\pi^-p$  reaction, obtained with the CLAS detector at Jefferson Laboratory. The measurements cover the invariant mass range of the final state hadrons from  $1.6 \text{ GeV} < W < 2.0 \text{ GeV}$ . For the first time the photocouplings of all prominent nucleon resonances in this mass range have been extracted from this exclusive channel. Photoproduction of two charged pions is of particular importance for the evaluation of the photocouplings for the  $\Delta(1620)1/2^-$ ,  $\Delta(1700)3/2^-$ ,  $N(1720)3/2^+$ , and  $\Delta(1905)5/2^+$  resonances, which have dominant decays into the  $\pi\pi N$  final states rather than the more extensively studied single meson decay channels.

*Keywords:* two pion photoproduction, resonance photocouplings, baryon state

*PACS:* 11.55.Fv, 13.40.Gp, 13.60.Le, 14.20.Gk

---

## 1. Introduction

Studies of the excitation spectrum of the nucleon and the resonance photocouplings from the experimental data on exclusive meson photoproduction represent an important avenue in the exploration of the strong interaction in the non-perturbative regime [1]. Evaluation of the excited nucleon spectrum within Lattice QCD [2], as well as within continuous QCD approaches [3], inform our understanding of relating the experimental results on the  $N^*$  spectrum to strong QCD dynamics and its emergence from the QCD Lagrangian. In the past decade, data on exclusive meson photoproduction of the nucleon have been obtained at CLAS, ELSA, MAMI, GRAAL, and LEPS [4, 5, 6, 7]. Much of the new data includes differential cross sections, and they include single-, double-, and triple-polarization asymmetries. This wealth of data provides for rigorous constraints on the reaction amplitudes that are necessary in order to potentially access the amplitudes for two-body final states such as  $\pi N$ ,  $\eta p$ ,  $\eta' p$ ,  $KY$ ,  $K^*Y$ , to constrain the  $\omega p$  and  $\phi p$  amplitudes, and to extend the knowledge on the reaction mechanisms for the double-meson channels  $\pi\pi N$  and  $\pi^0\eta N$ .

A global multi-channel analysis of these data by the Bonn-Gatchina group [8, 9] has provided strong evidence for several new baryon states that have been reported in the recent edition of the Review of Particle Properties (RPP) [10]. Strong evidence for the existence of the  $N(1895)1/2^-$  and  $N(1900)3/2^+$  resonances has recently become available [11]. In particular, the CLAS data in the  $KY$  channels [12, 13, 14, 15] has had a decisive impact on these findings. However, the  $\pi^+\pi^-p$  photoproduction data is also sensitive to new baryon states [2, 3, 16, 17] and offers another channel to search for such states. Nucleon resonances established in photoproduction can also be ob-

served in exclusive electroproduction off protons at different photon virtualities  $Q^2$ , with  $Q^2$ -independent masses and hadronic decay widths. This signature provides strong evidence for the existence of new states. Therefore, combined studies of the  $\pi^+\pi^-p$  photo- and electroproduction data available from CLAS [17, 18, 19] can potentially allow for the validation of the existence of missing baryon states in a nearly model-independent way. These studies have already revealed strong evidence for the existence of the new baryon state  $N'(1720)3/2^+$  [17].

Furthermore, the  $\pi^+\pi^-p$  channel is also a unique source of information on the photoproduction of several well-established resonances with masses above 1.6 GeV that decay preferentially into this channel. So far, the photocouplings of most  $N^*$  and  $\Delta^*$  states reported in the RPP were obtained from  $\pi N$  and multichannel photoproduction without data on  $\pi^+\pi^-p$  from a proton target. However, the two-body meson-baryon photoproduction channels have limited sensitivity to many of the resonances with masses above 1.6 GeV, making  $\pi\pi N$  photoproduction reactions the major source of information on their parameters. Moreover, the independent information from the  $\pi^+\pi^-p$  channel is critical in order to verify the results of other meson-baryon channels [20, 21]. Currently, exclusive photoproduction off nucleons with more than one meson in the final state has been explored much less than the two-body meson-baryon photoproduction channels.

In this paper we present the first data for the nine 1-fold differential  $\pi^+\pi^-p$  photoproduction cross sections off protons at  $W$  from 1.6 GeV to 2.0 GeV. These data have allowed us to determine the resonant contributions from a fit of all measured differential cross sections combined within the framework of the updated JM reaction model [20, 22, 23]. By employing a unitarized BW ansatz [20], the photocouplings of all prominent resonances with

masses above 1.6 GeV were extracted from the  $\pi^+\pi^-p$  photoproduction data for the first time.

## 2. Experiment

The data were collected using the CEBAF Large Acceptance Spectrometer (CLAS) [24] in Hall B at the Thomas Jefferson National Accelerator Facility during the “g11a” data taking period in 2004. The photons were produced by an unpolarized electron beam of 4.019 GeV energy incident upon a gold-foil radiator with a thickness of  $10^{-4}$  radiation lengths. The photon energies were determined by detecting post-bremsstrahlung electrons in the tagger counters of a tagging spectrometer [25]. The tagged-photon energy range was 20-95% of the electron beam energy. The tagged-photon beam impinged on a 40-cm-long LH<sub>2</sub> target. The temperature and pressure of this cryotarget were measured throughout the g11a run. The mean calculated density of H<sub>2</sub> was 0.0718 g/cm<sup>3</sup> with relative fluctuations of about 0.1% [26, 27].

The CLAS detector consisted of a series of detectors situated in six azimuthally symmetric sectors around the beamline. Three regions of drift-chambers (DC) [28] allowed for the tracking of charged reaction products in the toroidal magnetic field in the range of laboratory polar angles from 8° to 140°. A set of 342 time-of-flight scintillators (TOF) [29] was used to record the flight times of charged particles. Start Counter (ST) scintillators [30] surrounded the target cell and were used to determine the event start time. The trigger required a hit in the tagger in coincidence with ST and TOF hits in at least two of the six sectors of CLAS. During the g11a run period, the total number of triggers collected was  $\sim 2 \times 10^{10}$ , giving an integrated luminosity of 70 pb<sup>-1</sup>.

### 2.1. Event selection

We required the detection of at least two charged particles in CLAS. The event sample consisted of four topologies, one with all three final state hadrons detected and three others in which one out of the three final state hadrons was missing. For these events the momentum of the missing particle was reconstructed from energy-momentum conservation. The momenta of the reconstructed charged particles were corrected for energy loss in the target materials [31]. The tagged-photon energies were also corrected taking into account all known tagger focal plane deformations [32].

A kinematic fit was used for the event selection to isolate the  $\gamma p \rightarrow \pi^+\pi^-p$  reaction [33]. The events passing the kinematic fit with confidence level (CL) above 0.1 were accepted. The pull distributions of the measured kinematic quantities were reasonably fitted by Gaussians centered at  $0.00 \pm 0.05$  with  $\sigma = 1.0 \pm 0.1$ .

Some events passed the CL cut with one or more tracks assigned the wrong particle identity. To further clean up the event sample, we employed a timing cut  $|T_{tag} - T_{stt}| <$

1.5 ns, where  $T_{tag}$  is the vertex time of the incident photon measured by the tagger and  $T_{stt}$  is the vertex time of the final state particle measured by ST. The kinematic fit probed all matched photons, selecting the hit with the maximum CL value. The photon energy measured by the tagger was compared with the total energy computed from the four-momenta of the final state particles. This energy difference was found to be within  $\Delta E/E \approx 0.5\%$ , confirming the accuracy of the detector and photon beam calibrations and the purity of the final event sample.

The CLAS detector contained insensitive regions for particle detection. These insensitive regions were at the locations of the superconducting coils, as well as at forward ( $\theta < 4^\circ$ ) and backward angles ( $\theta > 140^\circ$ ) in the lab frame. Final state particles were selected to be within the “fiducial” regions with reliable particle detection efficiency, away from the insensitive regions. In addition, the kinematic regions where the particle detection efficiency was less than 5% were excluded. Overall  $\approx 400$  million  $\pi^+\pi^-p$  events were selected for the evaluation of the integrated and differential cross sections. An uncertainty of 3% for the event selection was determined from the mismatch between the fraction of selected  $\pi^+\pi^-p$  events in the kinematic fits of the Monte Carlo (MC) sample and the measured data.

### 2.2. Cross section evaluation

The  $\pi^+\pi^-p$  photoproduction by unpolarized photons off unpolarized protons at a given center of mass (CM) energy can be fully described by a 5-fold differential cross section. This cross section has a uniform distribution over the azimuthal CM angles for all final state hadrons. Integrating over the azimuthal CM angle allows the 5-fold differential cross section to be expressed as a 4-fold differential cross section.

The cross sections were defined using three sets of four kinematic variables. These included the permutations of the two invariant masses derived from pairing two of the three final state hadrons  $M_{ij}$  and  $M_{jk}$ , where  $i$ ,  $j$ , and  $k$  represent the final state particles  $\pi^+$ ,  $\pi^-$ , and  $p'$ . The definitions for the final state CM angular variables are given in Fig. 1. There are two relevant CM angles in each set of variables, 1)  $\theta_i$  for one of the final state hadrons  $i$  and 2)  $\alpha_{[ip][jk]}$  between the two hadronic planes defined by the three-momenta of the initial state proton  $p$  and the final state hadron  $i$ , and the three-momenta of the remaining final hadron pair  $jk$ . The reaction kinematics are described in detail in Refs. [21, 34].

The 4-fold differential cross sections were evaluated from the  $\pi^+\pi^-p$  event yields collected in the 4-dimensional (4-D) bins, normalizing by the detection efficiency in each bin and the overall beam-target luminosity. After integration of the 4-fold differential cross sections over the three different sets of three variables (see below), nine 1-fold differential cross sections were determined for 1.6 GeV  $< W < 2.0$  GeV in 25-MeV-wide  $W$  bins. These 1-fold differential cross sections include:

a) invariant mass distributions:

$$\frac{d\sigma}{dM_{\pi^+p'}}, \frac{d\sigma}{dM_{\pi^+\pi^-}}, \frac{d\sigma}{dM_{\pi^-p'}};$$

b) angular distributions over  $\theta$ :

$$\frac{d\sigma}{d(-\cos\theta_{\pi^-})}, \frac{d\sigma}{d(-\cos\theta_{\pi^+})}, \frac{d\sigma}{d(-\cos\theta_{p'})};$$

c) angular distributions over  $\alpha$ :

$$\frac{d\sigma}{d\alpha_{[\pi^-p][\pi^+p']}}, \frac{d\sigma}{d\alpha_{[\pi^+p][\pi^-p']}}, \frac{d\sigma}{d\alpha_{[p'p][\pi^+\pi^-]}}.$$

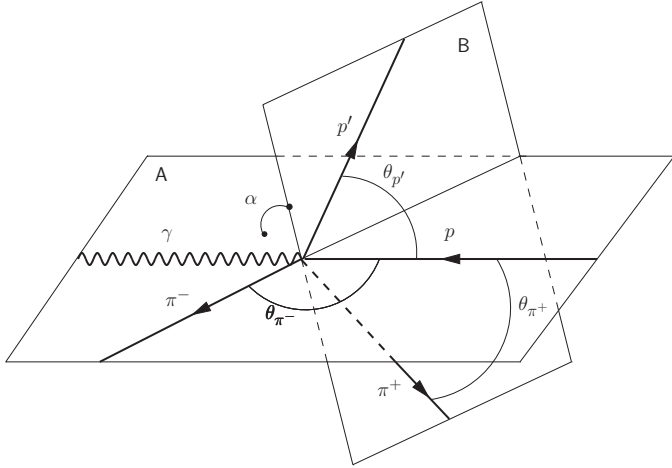


Figure 1: Angular kinematic variables for the reaction  $\gamma p \rightarrow \pi^+ \pi^- p'$  in the CM frame. The set with  $i=\pi^-$ ,  $j=\pi^+$ , and  $k=p'$  includes the angular variables for  $\theta_{\pi^-}$ , the polar angle of the  $\pi^-$ , and  $\alpha_{[\pi^-p][\pi^+p']}$ , which is the angle between the planes  $A$  and  $B$ , where plane  $A$  ( $[\pi^-p]$ ) is defined by the 3-momenta of the  $\pi^-$  and the initial state proton and plane  $B$  ( $[\pi^+p']$ ) is defined by the 3-momenta of the  $\pi^+$  and the final state proton  $p'$ . The polar angle  $\theta_{p'}$  is relevant for the set with  $i=p'$ ,  $j=\pi^+$ , and  $k=\pi^-$ , while the polar angle  $\theta_{\pi^-}$  belongs to the set with  $i=\pi^+$ ,  $j=p'$ , and  $k=\pi^-$ .

The detector efficiency was computed using a detailed GEANT simulation of the CLAS detector called GSIM [35] and an event generator based on the JM05 reaction model [36, 37]. Uncertainties related to the mismatch between the actual CLAS efficiency and that determined from the simulation were studied in Ref. [27] by comparing the yields of  $\omega$  electroproduction in the six sectors of CLAS. For experiments with unpolarized beam and target, all cross sections over the azimuthal angle should be uniform. The differences between the  $\omega$  yields in the different CLAS sectors was about 4%.

The evaluation of the CLAS detection efficiency was further checked through the comparison of the four integrals  $I$  of the normalized yields of the  $\pi^+\pi^-p$  events in the 4-D cells collected in the four different topologies (see Section 2.1) over the invariant masses  $M_{\pi^-p'}$  and  $M_{\pi^+\pi^-}$ , and the angle  $\alpha_{[p'p][\pi^+\pi^-]}$  (see Section 2.2). The integrals were calculated within the limited CLAS acceptance region where the 4-D cells contain the selected events of all four topologies. The four integrals  $I$  were obtained in each bin of  $W$  as a function of the CM angle  $\theta_{p'}$ . The deviation of the integrals from the four different topologies was about 4%. This variation was assigned as the systematic uncertainty for the detection efficiency (see Table 1). A

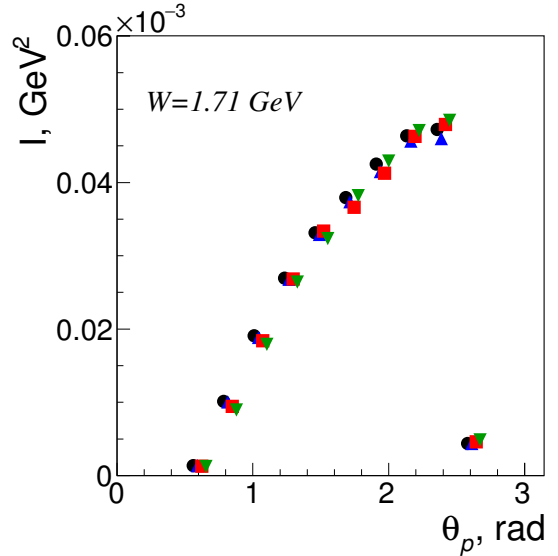


Figure 2: (Color Online) Representative integrals  $I$  over the variables  $M_{\pi^-p'}$ ,  $M_{\pi^+\pi^-}$ , and  $\alpha_{[p'p][\pi^+\pi^-]}$  as a function of  $\theta_{p'}$  at  $W=1.71$  GeV defined from the  $\pi^+\pi^-p$  normalized yields in the 4-D cells. The integrals contain only the 4-D cells where the events from all four topologies were available. Their values are shown as a function of  $\theta_{p'}$  for the four different topologies: all final state hadrons measured (black circles) and with the reconstructed momenta for the  $p'$  (red squares),  $\pi^-$  (blue triangles), and  $\pi^+$  (green upside down triangles). The integration over the two invariant masses gives integrals of dimension  $\text{GeV}^2$ .

representative example for comparison between the values of the four integrals is shown in Fig. 2.

The tagged photon flux on the target within the data acquisition live time was obtained by the standard CLAS *gflux* method [38]. The number of photons for each tagger counter was calculated independently as  $N_\gamma = \epsilon \cdot N_{e^-}$ , where  $N_{e^-}$  is the number of electrons detected by a tagger counter and  $\epsilon$  is the tagging ratio. The tagging ratio was determined by placing a total absorption counter (TAC) directly in the photon beam at low intensity and determining the ratio of the number of beam photons and the number of electrons detected in coincidence in the tagger. The global normalization uncertainty derived from the run-to-run variance and the estimated normalization variance with the electron beam current together were found to be 3.5%, employing the method described in Ref. [27].

In the determination of the fully-integrated and 1-fold differential cross sections, the contributions from the insensitive areas of CLAS were taken into account by extrapolating the 4-fold differential cross sections. As a starting point, the evaluation of the 1-fold differential cross sections in the full acceptance was carried out in the following way. The cross section values in each 1-D bin determined within the CLAS acceptance were multiplied by the ratio of the total number of 4-D bins that contributed to the analyzed one-dimensional (1-D) bin over the number of bins with non-zero efficiency.

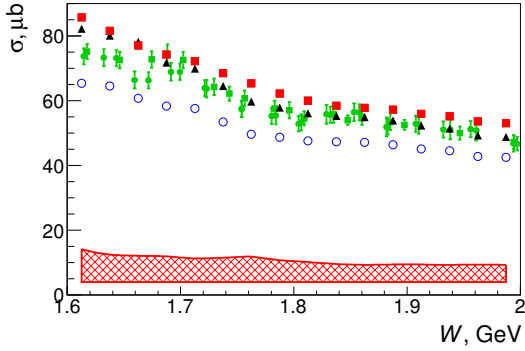


Figure 3: (Color Online) Fully integrated  $\pi^+\pi^-p$  photoproduction cross sections within the CLAS acceptance (blue open circles) and in the full acceptance after the initial 4-fold differential cross section extrapolation into the insensitive areas (black triangles) and after the improved extrapolation within the framework of the JM model as described in Section 2.2 (red squares). The CLAS data are compared with the SAPHIR [39] (green squares with error bars) and the ABBHHM [40] (green circles with error bars) results. The statistical uncertainties of our data are smaller than the marker size, while the systematic uncertainties are shown by the hatched area at the bottom of the figure.

An improved extrapolation of the 4-fold  $\pi^+\pi^-p$  differential cross sections into the insensitive areas of CLAS was carried out within the framework of the JM model [20, 22, 23]. The JM model parameters [20, 23] were fitted to the data within the CLAS acceptance and the 4-fold differential cross sections in the insensitive areas were computed from the JM model. Then, the JM model parameters were re-fitted to reproduce the cross sections determined in the full acceptance, obtained after filling the insensitive areas. The JM model with improved parameters was then used again for the evaluation of the cross sections in the insensitive areas of CLAS, generating a new set of differential cross sections extrapolated into the insensitive areas of CLAS. The uncertainties caused by the cross section extrapolation into the insensitive areas of CLAS were assigned as half the difference between the cross sections determined within the full and CLAS acceptances, which amounted to 12.0% for the integrated cross section. This uncertainty is strongly dependent on the CM polar angles of the final state hadrons. It was found that the two sets of nine 1-fold differential cross sections in the full acceptance agreed within the statistical uncertainties of the data.

Figure 3 shows the fully integrated cross section within the CLAS acceptance (blue circles). The other points are the cross sections corrected for acceptance by the two methods described above. The top panel of Fig. 4 shows a representative example of the initial and improved extrapolations for the 1-fold differential cross sections, where they are compared with the cross sections within the CLAS acceptance. In the bottom panel of Fig. 4, the improved extrapolated data obtained in the two steps of the JM

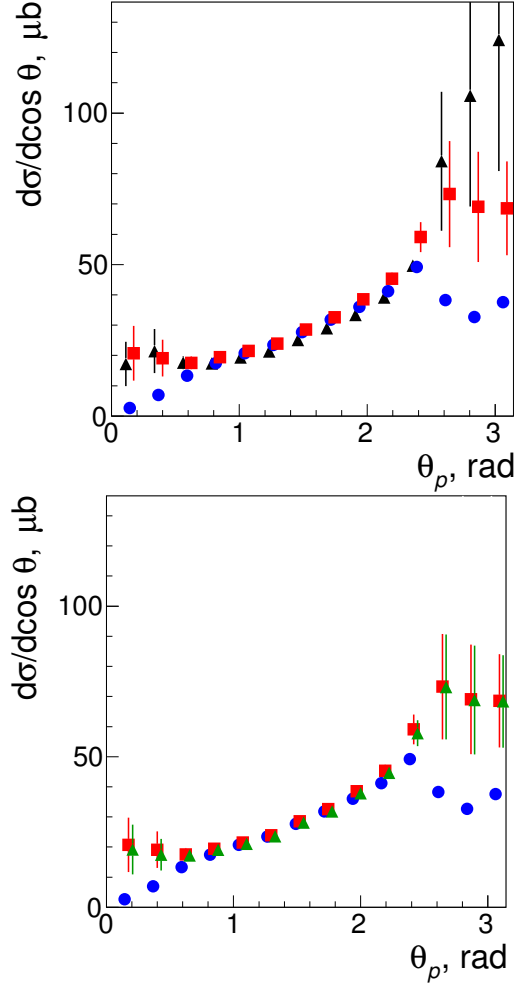


Figure 4: (Color Online) Representative  $\theta_{p'}$  angular distributions at  $W=1.71$  GeV. (Top) Results obtained within the CLAS acceptance (blue circles) and in the full acceptance extrapolating the cross section into the insensitive areas after the initial cross section extrapolation (black triangles) and the improved extrapolation using the JM model (red squares) as explained in Section 2.2. The error bars are dominated by the uncertainty of the extrapolation procedure. (Bottom) Results obtained within the CLAS acceptance (blue circles) and in the full acceptance (Section 2.2) obtained by extrapolating the cross section into the insensitive areas with the initial JM model parameters (green triangles) and after adjustment of the JM model parameters (red squares). The symbols have a small offset in  $\theta_{p'}$  for presentation purposes.

| Source of uncertainty                                | Contribution to fully integrated $\pi^+\pi^-p$ cross section, % |
|--|---|
| Fiducial area choice                                 | 4.0   |
| Event selection                                      | 3.0   |
| Run-to-run stability and global normalization factor | 3.5   |
| Efficiency from MC                                   | 4.0   |
| Impact of the CLAS insensitive areas                 | 12.0  |
| Total  | 14.0  |

Table 1: Summary of the systematic uncertainties for the fully integrated  $\pi^+\pi^-p$  photoproduction cross sections. The uncertainties estimated as the global multiplicative factors and point-by-point are listed in the second and third rows, respectively.

model data fit are presented.

The systematic uncertainties for the fully integrated  $\pi^+\pi^-p$  photoproduction cross sections are summarized in Table 1. The largest contribution comes from the 4-fold differential cross section extrapolation into the insensitive areas of CLAS. The systematic uncertainties related to the selection of the fiducial areas were estimated by comparing the cross sections computed with two different minimum CLAS detection efficiency cuts: 5% (nominal) and 10% (increased). The 4-fold differential cross section inside the excluded areas with small detection efficiency were estimated within the extrapolation procedure described above. The computed cross sections with the increased and nominal detection efficiency cuts differ by about 4% as listed in Table 1.

### 3. Results and Physics Analysis

The fully integrated  $\pi^+\pi^-p$  photoproduction cross section and representative examples of the nine 1-fold differential cross sections are shown in Fig. 3, Fig. 5, and Fig. 6, respectively. We show the differential cross sections in a  $W$ -bin centered at 1.74 GeV, which corresponds to the peak of the resonance-like structure observed in the  $W$ -dependence of the  $\pi^+\pi^-p$  electroproduction cross sections [18]. The complete set of differential cross sections from this experiment can be found in the CLAS physics database [41]. The error bars for the cross sections shown in Figs. 5 and 6 include the uncertainties related to the extrapolation of the 4-fold differential cross sections into the inefficient areas of CLAS. The fully integrated cross sections from CLAS are consistent with the existing results within the systematic uncertainties [39, 40]. However, our fully integrated cross sections in the full acceptance are slightly above the existing results likely due to the different approaches used for the cross section extrapolations into the inefficient areas. We consider estimates of the 5-fold differential cross sections in the inefficient areas from the updated JM16 model, outlined below, as reliable, since the

nine 1-fold differential cross sections are well described by the JM16 model within the acceptance as shown in Figs. 5 and 6.

The nucleon resonance photocouplings in the mass range from 1.6 GeV to 2.0 GeV were determined from a fit to all nine 1-fold differential cross sections from  $\pi^+\pi^-p$  photoproduction. The fit was performed within the framework of the JM16 model updated to describe the  $\pi^+\pi^-p$  photoproduction data. Previously, the JM model was successfully used for the extraction of the nucleon resonance couplings from the CLAS  $\pi^+\pi^-p$  electroproduction data [20, 21, 22, 23, 37]. This approach provided electrocouplings for the  $N(1440)1/2^+$  and  $N(1520)3/2^-$  from this channel that were published in the latest RPP edition [10]. The JM16 model incorporates all mechanisms that contribute to  $\pi^+\pi^-p$  photoproduction in the resonance region with manifestations seen in the measured differential cross sections. These consist of the  $\pi^-\Delta^{++}$ ,  $\pi^+\Delta^0$ ,  $\rho^0p$ ,  $\pi^+N(1520)3/2^-$ , and  $\pi^+N(1685)5/2^+$  meson-baryon channels, as well as the direct production of the  $\pi^+\pi^-p$  final state without formation of intermediate unstable hadrons. The modeling of these processes was described in Refs. [20, 22, 23, 36, 37].

The  $\pi^+\pi^-p$  photoproduction data at  $W > 1.8$  GeV require implementation of the  $\sigma p$  meson-baryon channel, which was parameterized by a 3-body contact term and an exponential propagator for the intermediate  $\sigma$  meson. The magnitudes of the parameterized  $\sigma p$  photoproduction amplitudes were fitted to the data in each bin of  $W$  independently. The contributions from well established  $N^*$  states with masses  $< 2.0$  GeV and observed decays to the  $\pi\pi N$  final states were included into the  $\pi\Delta$  and  $\rho p$  meson-baryon channels of JM16. The resonant amplitudes were described in a unitarized Breit-Wigner ansatz [20] that accounted for restrictions imposed by a general unitarity condition to the resonant contributions [42]. The JM16 model reproduces well the  $\pi^+\pi^-p$  differential cross sections at  $W < 2.0$  GeV (see Fig. 5), with a  $\chi^2$  per data point ( $\chi^2/d.p$ ) in individual  $W$ -bins less than 1.4, with the resonance photocouplings taken from the PDG and the total and partial resonance decay widths to the  $\pi\pi N$  final states taken from the previous analyses of the CLAS  $\pi^+\pi^-p$  electroproduction data [23, 43].

As shown in Fig. 5, the individual contributing mechanisms have distinctive differences in the shapes in all nine 1-fold differential cross sections. Furthermore, the shape of the cross section for each meson-baryon channel changes considerably in the different 1-fold differential cross sections. These changes are determined by the underlying reaction dynamics. Therefore, the successful reproduction of the measured cross sections within the JM16 model provides confidence that this model incorporates all essential contributing mechanisms and offers a reasonable description of these mechanisms.

In the data fit, the resonance photocouplings, the  $\pi\Delta$  and  $\rho p$  decay widths, the parameters of the non-resonant amplitudes described in Refs. [20, 21], and the magnitudes

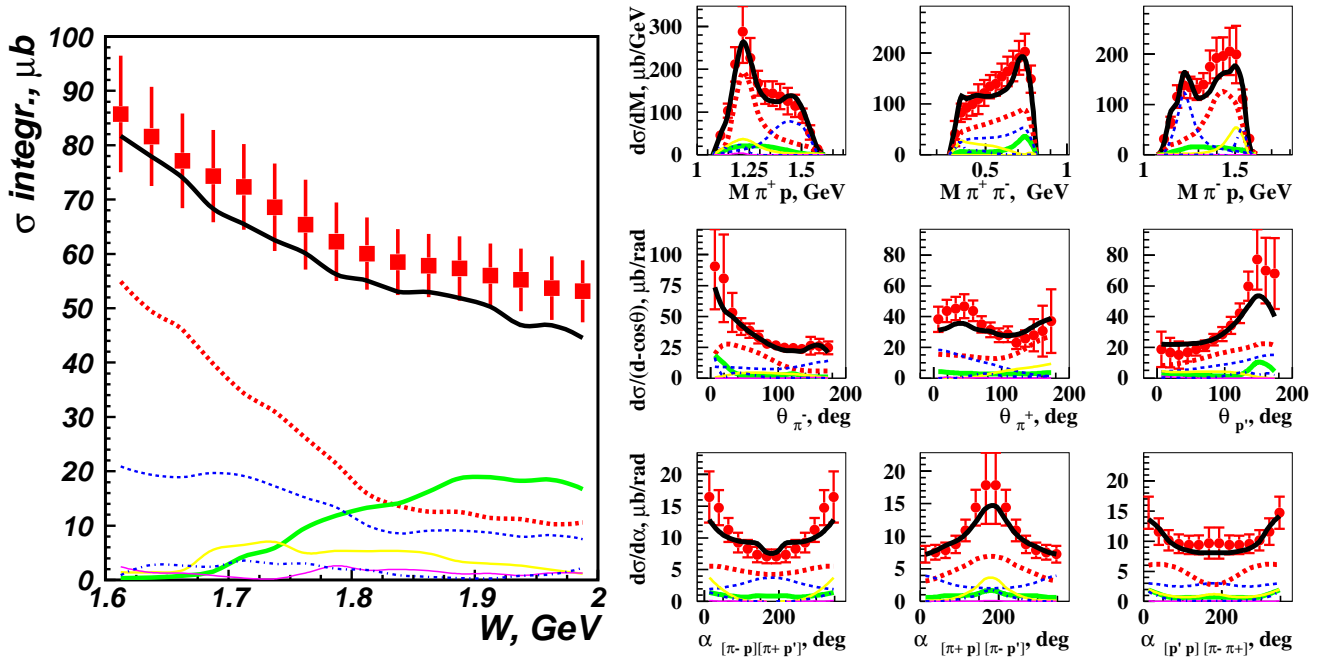


Figure 5: (Color Online) Description of the  $\pi^+\pi^-p$  photoproduction cross sections and the contributions from the relevant channels inferred from the CLAS data within the framework of the JM16 model for the fully integrated cross sections (left) and a representative example of the nine 1-fold differential cross sections at  $W=1.74$  GeV (right) shown by different lines: full reaction cross sections (thick black),  $\pi^-\Delta^{++}$  (red dashed thick),  $pp$  (green thick),  $\pi^+\Delta^0$  (blue dashed),  $\pi^+N(1520)3/2^-$  (yellow),  $2\pi$ -direct production (magenta), and  $\pi^+N(1685)5/2^+$  (blue dot-dashed). The error bars include uncertainties related to the 4-fold differential cross section extrapolation into the inefficient areas of CLAS.

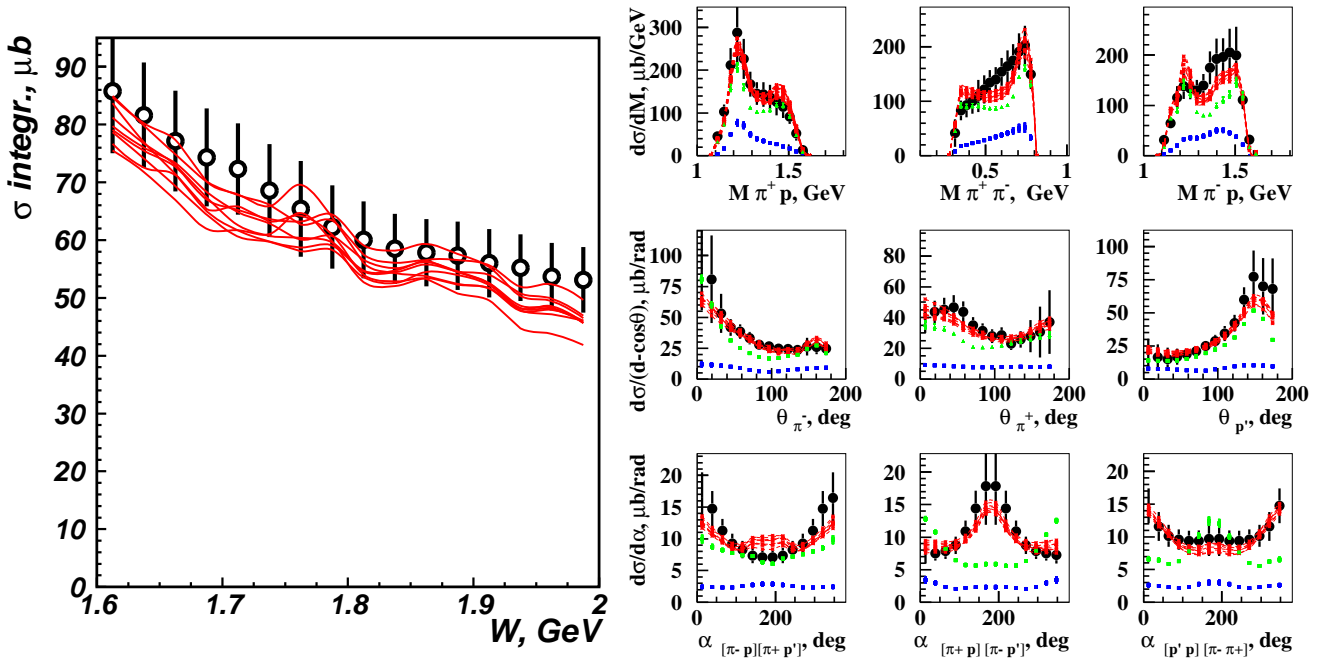


Figure 6: (Color Online) (Left) Fully integrated cross sections from the fits of the nine 1-fold differential cross sections (curves) in comparison with the measured integrated cross section. The error bars include uncertainties related to the 4-fold differential cross section extrapolation into the inefficient areas of CLAS. (Right) Resonant/non-resonant contributions to the nine 1-fold differential cross sections from the fit of the CLAS  $\pi^+\pi^-p$  photoproduction data within the framework of the JM16 model at  $W=1.74$  GeV. The computed cross sections are shown by the red curves, while the resonant/non-resonant contributions inferred from the fit are shown by the blue/green bars, respectively.

| Resonances          | $A_{1/2} \times 10^3$<br>from $\pi^+\pi^-p$<br>GeV $^{-1/2}$ | $A_{3/2} \times 10^3$<br>from $\pi^+\pi^-p$<br>GeV $^{-1/2}$ | $A_{1/2} \times 10^3$<br>from $\pi N$<br>GeV $^{-1/2}$ | $A_{3/2} \times 10^3$<br>from $\pi N$<br>GeV $^{-1/2}$ |
|---------------------|--|--|--|--|
| $\Delta(1620)1/2^-$ | $29.0 \pm 6.2$   |  | $27 \pm 11^*$  |  |
| $N(1650)1/2^-$      | $60.5 \pm 7.7$   |  | $45 \pm 10^*$  |  |
| $N(1680)5/2^+$      | $-27.8 \pm 3.6$  | $128 \pm 11$   | $-15 \pm 6^*$  | $133 \pm 12^*$   |
| $N(1720)3/2^+$      | $80.9 \pm 11.5$  | $-34.0 \pm 7.6$  | $91 \pm 3^{**}$  | $-36 \pm 4^{**}$                                       |
| $N'(1720)3/2^+$     | $36.5 \pm 6.3$   | $-39.6 \pm 6.8$  |  |  |
| $\Delta(1700)3/2^-$ | $87.2 \pm 18.9$  | $87.2 \pm 16.4$  | $104 \pm 15^{***}$                                     | $85 \pm 22^{***}$                                      |
| $\Delta(1905)5/2^+$ | $19.0 \pm 7.6$   | $-43.2 \pm 17.3$   | $22 \pm 5^*$   | $-45 \pm 10^*$   |
| $\Delta(1950)7/2^+$ | $-69.8 \pm 14.1$   | $-118.1 \pm 19.3$  | $-76 \pm 12^{***}$                                     | $-97 \pm 10^{***}$                                     |

Table 2: Resonance photocouplings determined from analysis of the  $\pi^+\pi^-p$  photoproduction data from this work in comparison with the previous results from the RPP-16 [10] (\*), CLAS data on  $\pi N$  photoproduction [45] (\*\*) and RPP-12 [46]. The candidate  $N'(1720)3/2^+$  state seen in analyses of  $\pi^+\pi^-p$  photo-/electroproduction data [17] and included in the fit is highlighted in it alics.

of the  $\sigma p$  photoproduction amplitudes were varied independently around their initial values. The initial values for the  $\pi\Delta$  and  $\rho p$  decay widths were taken from analyses of the previous CLAS  $\pi^+\pi^-p$  electroproduction data [23, 43] for resonances with masses up to 1.8 GeV. For heavier  $N^*$  we used the results of Refs. [10, 44]. The initial resonance photocouplings were taken Refs. [10, 17, 45]. In order to describe the CLAS  $\pi^+\pi^-p$  photo- and electroproduction data at  $W \approx 1.7$  GeV with  $Q^2$ -independent mass and hadronic decay widths of the contributing resonances, the new  $N'(1720)3/2^+$  baryon state is needed. It was included in the data fit with the photo- and hadronic couplings starting from the values in Ref. [17]. The initial values for the JM16 resonant and non-resonant parameters were further adjusted to reproduce the  $\pi^+\pi^-p$  photoproduction data. The resonant/non-resonant parameters were sampled around their initial values, employing unrestricted normal distributions with a width ( $\sigma$ ) of magnitude 30% of the initial value. For each trial set of the resonant and non-resonant parameters, we computed the nine 1-fold differential  $\pi^+\pi^-p$  cross sections and estimated the  $\chi^2/d.p.$  values in point-by-point comparisons. We selected the computed 1-fold differential cross sections closest to the data with  $\chi^2/d.p.$  determined from a fit to the entire  $W$ -range from 1.6 GeV to 2.0 GeV. We required  $\chi^2/d.p.$  to be less than a maximum value of 1.31, which amounted to requiring that the computed cross sections be within the data uncertainties.

Selected computed differential cross sections together with the resonant/non-resonant contributions are shown in Fig. 6. The uncertainties for the resonant contributions are comparable with those for the experimental data, suggesting credible and unambiguous access to the resonant contributions in the differential cross sections. The resonance photocouplings were inferred from the resonant contributions by employing a unitarized Breit-Wigner ansatz [20]. The differences of the resonant and non-resonant contributions (see Fig. 6) in the nine 1-fold differential cross sections, in particular in the CM angular distributions,

allows clean resonance photocoupling extraction even in bins where the latter is a small contribution. The resonance parameters assigned in the computed cross sections selected in the fit were averaged and their mean values were taken as the extracted resonance parameters. The dispersion in these parameters was taken as the associated systematic uncertainty. The resonance photocouplings extracted from this work are listed in Table 2 and compared with the previous results from  $\pi N$  photoproduction data and multichannel analyses from Refs. [10, 45]. There is a good agreement in the magnitude and the photocoupling sign between previous data and our results.

#### 4. Summary

The first results on nine independent 1-fold differential and fully integrated  $\pi^+\pi^-p$  photoproduction cross sections off protons in the range of  $W$  from 1.6 GeV to 2.0 GeV have become available from measurements with the CLAS detector at Jefferson Lab. Using the updated JM meson-baryon reaction model, these data have allowed us to establish all essential contributing mechanisms from their manifestations in the measured observables. The resonant contributions were deconvoluted by using fits to the experimental data, comprising nine 1-fold differential cross sections measured with CLAS. The good description of the experimental data achieved in the entire  $W$  range provides confidence in the reliability of our extraction of the nucleon resonance and background contributions. This is supported by the comparable uncertainties for the measured differential cross sections and the resonant/non-resonant contributions extracted from the data fit.

Using a unitarized Breit-Wigner ansatz [20], which allowed us to account for the restrictions imposed by a general unitarity condition on the resonant amplitudes, the resonance photocouplings were determined from the resonance contributions. For the first time, the nucleon resonance photocouplings for the states in the mass range from 1.6 GeV to 2.0 GeV were determined from analysis of

the data on  $\pi^+\pi^-p$  photoproduction. The  $\Delta(1620)1/2^-$ ,  $\Delta(1700)3/2^-$ ,  $N(1720)3/2^+$ , and  $\Delta(1905)5/2^+$  resonance photocouplings were extracted from the  $\pi^+\pi^-p$  photoproduction channel with much improved confidence over any previous analysis, because of the preferential decays of these resonances to the  $\pi\pi N$  final states with branching fractions above 70%. This work is now the major source of information on the photocouplings of these states. The results on the  $N^*$  photocouplings from  $\pi^+\pi^-p$  photoproduction show good consistency with previous  $\pi N$  and multichannel analyses, which is an important result considering the very different background processes in the  $\pi^+\pi^-p$  channel in comparison with the previously studied exclusive channels. This work establishes the capability to reliably extract resonance photocouplings and helps to validate the procedure for resonance parameter extraction employed in the JM16 model. The results presented in the paper pave the way for the future combined analysis of the  $\pi^+\pi^-p$  photo- and electroproduction data from CLAS, which has already revealed further substantial evidence for the new  $N'(1720)3/2^+$  baryon state [17].

## 5. Acknowledgments

We would like to acknowledge the outstanding efforts of the staff of the Accelerator and the Physics Divisions at Jefferson Lab that made this experiment possible. This work was supported in part by the Chilean Comisión Nacional de Investigación Científica y Tecnológica (CONICYT), the Italian Istituto Nazionale di Fisica Nucleare, the French Centre National de la Recherche Scientifique, the French Commissariat à l'Énergie Atomique, the U.S. Department of Energy, the National Science Foundation, the Scottish Universities Physics Alliance (SUPA), Skobeltsyn Institute of Nuclear Physics, the Physics Department at Moscow State University, Ohio University, the University of South Carolina, the United Kingdom's Science and Technology Facilities Council (STFC), and the National Research Foundation of Korea. The Southeastern Universities Research Association (SURA) operates the Thomas Jefferson National Accelerator Facility for the United States Department of Energy under contract DE-AC05-84ER40150. This material is based upon work supported by the U.S. Department of Energy, Office of Science, Office of Nuclear Physics under contract DE-AC05-06OR23177.

## References

- [1] I.G. Aznauryan *et al.*, Int. J. Mod. Phys. **E22**, 1330015 (2013).
- [2] J.J. Dudek and R.G. Edwards, Phys. Rev. D **85**, 054016 (2012).
- [3] H.L.L. Roberts *et al.*, Few Body Syst. **51**, 1 (2011).
- [4] V. Crede and W. Roberts, Rep. Prog. Phys. **76**, 076301 (2013).
- [5] V.D. Burkert, EPJ Web Conf. **37**, 01017 (2012).
- [6] V.D. Burkert, Few Body Syst. **57**, 873 (2016).
- [7] A.V. Anisovich *et al.*, Eur. Phys. J. **A52**, 284 (2016).
- [8] A.V. Anisovich *et al.*, Eur. Phys. J. **A48**, 15 (2012).
- [9] A.V. Anisovich *et al.*, Eur. Phys. J. **A50**, 129 (2014).
- [10] C. Patrignani *et al.* (Particle Data Group), Chin. Phys. C **40**, 100001 (2016).
- [11] A.V. Anisovich *et al.*, Eur. Phys. J. **A53**, 242 (2017).
- [12] R.K. Bradford *et al.* (CLAS Collaboration), Phys. Rev. C **73**, 035202 (2006).
- [13] R.K. Bradford *et al.* (CLAS Collaboration), Phys. Rev. C **75**, 035205 (2007).
- [14] M.E. McCracken *et al.* (CLAS Collaboration), Phys. Rev. C **81**, 025201 (2010).
- [15] B. Dey *et al.* (CLAS Collaboration), Phys. Rev. C **82**, 025202 (2010).
- [16] S. Capstick and W. Roberts, Prog. Part. Nucl. Phys. **45**, S241 (2000).
- [17] V.I. Mokeev *et al.*, EPJ Web Conf. **113**, 01013 (2016).
- [18] M. Ripani *et al.* (CLAS Collaboration), Phys. Rev. Lett. **91**, 022002 (2003).
- [19] E.L. Isupov *et al.* (CLAS Collaboration), Phys. Rev. C **96**, 025209 (2017).
- [20] V.I. Mokeev *et al.* (CLAS Collaboration), Phys. Rev. C **86**, 055203 (2012).
- [21] V.I. Mokeev *et al.*, Phys. Rev. C **93**, 054016 (2016).
- [22] V.I. Mokeev *et al.*, Phys. Rev. C **80**, 045212 (2009).
- [23] V.I. Mokeev, Few Body Syst. **57**, 909 (2016).
- [24] B.A. Mecking *et al.*, Nucl. Instr. and Meth. **A503**, 513 (2003).
- [25] D. I. Sober *et al.*, Nucl. Instrum. Meth. A **440**, 263 (2000).
- [26] R. Bradford and R.A. Schumacher. CLAS-Note 2002-003, [https://www.jlab.org/Hall-B/notes/clas\\_notes02/02-003.pdf](https://www.jlab.org/Hall-B/notes/clas_notes02/02-003.pdf).
- [27] M. Williams, Carnegie Mellon University Ph.D. Thesis, (2007).
- [28] M.D. Mestayer *et al.*, Nucl. Instr. and Meth. **A449**, 81 (2000).
- [29] E. Smith *et al.*, Nucl. Instr. and Meth. **A432**, 265 (1999).
- [30] Y. Sharabian *et al.*, Nucl. Instr. and Meth. **A559**, 246 (2006).
- [31] E. Pasyuk, CLAS-Note 2007-016, <https://misportal.jlab.org/ul/Physics/Hall-B/clas/viewFile.cfm/2007-016.pdf?documentId=423>.
- [32] S. Stepanyan *et al.*, Nucl. Instrum. Meth. A **572**, 654 (2000).
- [33] M. Williams and C.A. Meyer, CLAS-Note 2003-017, [https://www.jlab.org/Hall-B/notes/clas\\_notes03/03-017.pdf](https://www.jlab.org/Hall-B/notes/clas_notes03/03-017.pdf).
- [34] G.V. Fedotov *et al.* (CLAS Collaboration), Phys. Rev. C **79**, 015204 (2009).
- [35] M. Holtrop, [http://nuclear.unh.edu/~maurik/gsim\\_info.shtml](http://nuclear.unh.edu/~maurik/gsim_info.shtml).
- [36] M. Ripani *et al.*, Nucl. Phys. A **672**, 220 (2000).
- [37] I.G. Aznauryan *et al.*, Phys. Rev. C **72**, 045201 (2005).
- [38] J. Ball and E. Pasyuk, CLAS-Note 2005-002, <https://misportal.jlab.org/ul/Physics/Hall-B/clas/viewFile.cfm/2005-002.pdf?documentId=24>.
- [39] C. Wu *et al.*, Eur. Phys. J. A **23**, 317 (2005).
- [40] ABBHHM Collaboration, Phys. Rev. **188**, 2060 (1969).
- [41] CLAS Physics Database <https://clasweb.jlab.org/physicsdb/>.
- [42] I.J.R. Aitchison, Nucl. Phys. A **189**, 417 (1972).
- [43] V.I. Mokeev and I.G. Aznauryan, Int. J. Mod. Phys. Conf. Ser. **26**, 146080 (2014).
- [44] D.M. Manley and E.M. Salesky, Phys. Rev. D **45**, 4002 (1992).
- [45] M. Dugger *et al.* (CLAS Collaboration), Phys. Rev. C **79**, 065206 (2009).
- [46] J. Beringer *et al.* (Particle Data Group), Phys. Rev. D **86**, 010001 (2012).